CALCULATION OF PROTON INDUCED REACTION CROSS SECTIONS OF LONG-LIVED FISSION PRODUCTS USING EMPIRE CODE

T. S. Longmena[1], O.O. Ige[2*], G.J. Ibeh[2] and S.A. Jonah[3]

[1]Federal College of Education, Pankshin, Nigeria.
[2]Department of Physics, Nigerian Defence Academy, Kaduna, Nigeria.
[3]Centre for Energy Research and Training, Ahmadu Bello University, Zaria, Nigeria.

ABSTRACT

A systematic theoretical investigation of the excitation function of the Long-Lived Fission Products (LLFPs); which are problematic radioactive wastes in spent nuclear fuels; was performed with the aim of determining an optimal strategy for their transmutation in Accelerator Driven System (ADS)as a special technique for safe management and disposal. The (p,n), (p,2n), and (p,3n) reactions cross sections of some of the LLFPs, resulting in the transmutation to their short-lived or stable progenies, were calculated using EMPIRE-3.2atproton incident energy up to 200MeV with selected model and parameter considerations covering the Optical (OM), Compound Nucleus (CN) and Preequilibrium (PE) mechanisms. Dispersive and Relativistic consideration of the optical wave represented in the Optical Model Potential (OMP) were found to have no impact on the description of the Direct Reaction cross section from the OM. The PE model was best described with the HMS mechanism especially above 30 MeV while increasing the Mean Free Path (MFP) to 3.0 improved the contribution of the PCROSS mechanisms especially in reducing the peak cross section to reproduce available measured data. For transmutation application, the peak characteristics of Cross Section at Corresponding Energy is reported for this work as 468.33 ± 198.67 mb at 9.99 ± 0.06 MeV for (n,p) reactions; 935.82 ± 99.69 mb at 18.79 ± 2.36 MeV for (n,2p) reaction and 709.48 ± 222.20 mb at 28.89 ± 2.41 MeV for (n,3p) reactions. Overall, the calculated cross sections, compares well with the scanty available measured data from the EXFOR data Library and the TENDL evaluated data files and showed good agreement within the region of relevant application. It shows clear improvement of the peak cross section region of the neutron emission spectrum and thus better features of nuclei decay than the data from TENDL 2009 and TENDL 2014.

Key words:
Cross section, Long-Lived Fission Products, Accelerator Driven System, Transmutation, Proton induced reaction.

Corresponding author's e-mail: ooige@nda.edu.ng *website: www.academyjsekad.edu.ng*

1.0 INTRODUCTION

Long-lived Fission Products (LLFPs), such as ^{79}Se, ^{93}Zr, ^{99}Tc, ^{107}Pd, ^{126}Sn, ^{129}I and ^{135}Cs, constitute a significant waste burden from nuclear power plant. These LLFPs dominate the long-term dose associated with radionuclide release from High Level Waste (HLW) and geological repositories (Yang et al., 2004, Satoshi, 2017). For sustainable nuclear energy programmes, the management of such long-lived nuclear waste is very critical both for the practical long-term reactor safety and security strategy and the improvement of public perception and acceptance of nuclear power generation.

Partitioning and Transmutation, (P&T), carried out on the spent fuel before disposal, has been proposed as a candidate strategy to minimize the risk associated with the long-term disposal of HLW in well evaluated geological repositories. The main aim of P&T is to reduce the long-term radiotoxic inventory of the waste, making its disposal safer and alleviating the uncertainties associated with the long-term scale management. This is achieved by chemical separation of the spent fuel to isolate those requiring transmutation and subsequently, through radionuclide conversion, transform the isolated long-lived radioactive isotopes into short-lived or even stable ones(European Commission, 2001). P&T also aims at reducing the volume of waste requiring deep geological disposal; hence the associated space requirements and thereby the eventual economic considerations for such repositories.

Recently, the use of Accelerator Driven System (ADS) for HLW transmutation has been promoted and is currently receiving increased attention due to its potential to improve the flexibility and safety characteristics of transmutation. The ADS, a subcritical nuclear reactor system, is designed as a coupling of a substantially subcritical core with a high-energy proton accelerator and could use more abundant Thorium as a fuel in place of the less abundant Uranium while producing shorter lived nuclide in less quantity in the HLW inventory(IAEA, 2015).Thus, the large flexibility provided by the ADS has opened up viable considerations of a highly efficient new energy production concept with potential ways to destroy or reduce the radioactivity and radiotoxicity of the HLW thereby opening up consideration for surface disposal within a period of time comparable with human lifetime (Ikeda, 2014).It however requires improved set of consistent, precise and accurate nuclear data for it designs, implementation and operation and global studies towards achieving this aim are underway (Makinaga et al., 2014).

From the viewpoint of nuclear data, different kinds of cross section data for LLFPs are needed in significant quantity and over an extended energy range to design and operate the nuclear transmutation system reliably and efficiently while considering costs (Makinaga et al., 2014).In this scenario

nuclear reaction information becomes the starting point of further serious computational modeling of a realistic ADS design which must involve nuclear reactions with incident particle energy of the order of GeV required for spallation processes.

This sort of full understanding of the nuclear process of the system is therefore the baseline for establishing the system concept and developing the engineering design where requirement for more detail description of nuclear products is paramount. Nuclear data is needed for a wide range of energy and materials different from those of fission or fusion reactors.

Very scanty measured and evaluated data have been reported for the (p,n), (p,2n) and (p,3n) reactions channels of LLFPs in the standard EXFOR library, the ENDF library and in other extant literature. Available measurement include Wang *et al.* (2016) who reported 2.15 ± 0.249 mb for ^{90}Sr(p,n) ^{90}Y, 12.1 ± 0.551 mb for ^{90}Sr(p,2n)^{89}Y and 16.1 ± 0.649 mb for ^{90}Sr(p,3n)^{88}Y all at 185MeV/A proton energy of an accelerator. Also, in the same study, 71.2 ± 7.14 mb was reported for ^{157}Cs(p,2n)^{136}Ba and 83.9 ± 6.01 mb for ^{157}Cs(p,3n)^{135}Baat 185MeV/A. Meanwhile, Zaytseva *et al.(*1992) reported the cross section of ^{99}Tc(p,3n) reaction from 20.7 MeV to 99.5MeV with cross section data increasing from 9.0 mb to 41.0 mb.

Only (p,2n) and (p,3n) reaction channels have been reported in evaluated data libraries and literature. In the ENDF Library, Shubin et al.,(1995) reported these two channels in MENDL – 2 and Koning and Rochman (2012) in both TENDL 2009 and TENDL 2014. There are no reports of evaluations for (n,p) reaction channel for LLFPs. The available evaluated data for these (p,2n) and (p,3n) also lacks poor description of the energy region of the neutron emission spectrum.

Therefore, in this work the reaction cross sections of (p,n), (p,2n), and (p,3n) for the transmutation of the LLFPs to short live or stable nuclides have been calculated using EMPIRE-3.2 nuclear reaction code for incident proton energy up to 200MeV

2.0 MATERIALS AND METHOD

For this work, EMPIRE 3.2 (Malta) installed in a Fedora 16 OS was used. Model considerations includes the OM, CN model and the PE model while other reaction ingredients and parameters were tested and studied including different OMPs.

For the Spherical Optical Model (SOM), the total cross section, which takes into account all flux lost from the incident plane wave either by scattering or by absorption, is defined as the sum of the elastic and reaction (or absorption) cross section (Raynal, 1972), and given as

$$\sigma_T = \sigma_E + \sigma_R = \frac{\pi}{k^2}\sum_{lj}(2j+1)\left(1 - ReS_l^j\right) \quad [1]$$

For the Coupled Channel Optical Model (CCOM) the total cross section which takes into account the occurrence of scattering of any type and is a measure of the flux lost from the incident plane wave state (Soukhovitskii et al., 2004;Soukhovitskii et al., 2005; Soukhovitskii et al., 2008) is described by

$$\sigma_T = \sigma_E + \sigma_R = \frac{1}{2I_0+1}\frac{\pi}{k^2}\sum_{ljJ}(2J+1)\left(1 - ReS^J_{ljc_0,ljc_0}\right) \quad [2]$$

In implementing [2] the usual standard phenomenological empirical potentials in a functional form involving only a limited set of parameters adjustable to obtain a best fit with experimental data has been used (Carlson, 2002). This Optical Model Potential (OMP), which evolved over the years, permits the parametrization of the scattering of a light particle such as neutron, proton, deuteron, tritium, or alpha, from a given nucleus and is given as Equation [3].

$$\begin{aligned} V(r_o) &= +Vc(r) - (V + iW) fv, w(r) + (V_s - iW_s) gv, w_s(r) \\ &- d_{so}\vec{l}.\vec{s}(V_{so} + iW_{so}) hv_{so,} w_{so}(r) \end{aligned} \quad [3]$$

Here, the first term is the coulomb term, second term is the complex volume term, third term is the complex surface term, the fourth term is the complex spin-orbit term; m_π is the Pion mass and d_{so} is the spin orbit constant. Different phenomenological descriptions of the OMP, including Relative and Dispersive considerations, selected from the Reference Input Parameter Library 3 (RIPL-3), were tested in this study namely Koning and Delaroche (2003); Morillon and Romain (2007) and Xiaohua and Chonghai (2008).

Table 1: List of tested Optical Model Parameters

Lib. No	Incident Particle	Model Type	Dispersive Potential	Relative Potential	Z-Range	A-Range	E-Range	Reference
5405	p	Spherical	no	yes	13 - 83	27- 209	0 - 200	Koning& Delaroche (2003)
5410	p	Spherical	yes	yes	13 - 83	27 -209	0 - 200	Morilon& Romain (2007)
5411	p	Spherical	yes	yes	13 - 83	27 -209	0 - 200	Morilon & Romain (2007)
5501	P	Spherical	yes	no	12 - 94	24 -240	0 - 200	Xiaohua& Chongai (2008)

Furthermore, two PE model namely the exciton (PCROSS) and the Hybrid Monte Carlo Simulation (HMS) models have been considered and used in modeling. For the PCROSS exciton model (Capote, et al., 1991) the PE spectra was calculated as:

$$\frac{d\sigma_{p,x}}{d\epsilon_x}(\epsilon_x) = \sigma^r_{p,x}(E_{inc})D_{p,x}(E_{inc}) \times \sum_n W_x(E,n,\epsilon_x)\tau(n) \quad [4]$$

Here,$\sigma^r_{p,x}(E_{inc})$ is the cross section of the reaction, (p,x),$W_x(E,n,\epsilon_x)$ is the probability of emission of a particle of type x or gamma ray with energy$\epsilon_x$from a state with n excitons and excitation energy E of the compound nucleus. Also$D_{p,x}(E_{inc})$is the depletion which takes into account the flux loss as a result of the direct reaction cross section processes. This depletion factor was calculated using the direct reaction cross section as

$$D_{p,x}(E_{inc}) = 1 - \frac{\sigma^{dir}_{p,x}(E_{inc})}{\sigma^r_{p,x}(E_{inc})} \quad [5]$$

The HMS PE model (Chadwick, et al., 1994), in which linear momentum conservation is included has been considered. It treats all excitons, including holes, on equal footings, giving each of them a chance to interact or to be emitted with a priori equal probability and ending the cascade when all excitons are bound. It gives the emission probability $P_\nu(E)$ as

$$P_\nu(E-Q) = \frac{\lambda_c(\varepsilon-Q)}{\lambda_c(\varepsilon-Q)+\lambda_+(\varepsilon)} \quad [6]$$

Where the emission rate $\lambda_c(\varepsilon - Q)$is given as

$$\lambda_c(\varepsilon - Q) \sim \frac{\sigma_\upsilon(\varepsilon-Q)(\varepsilon-Q)(2S+1)\mu_\nu}{g} \quad [7]$$

Here, $\sigma_\upsilon$gives the inverse reaction cross section, Qgives the binding energy, g is the single particle density, S is the nucleon Spin, $\mu_s$is the reduced nucleon mass and$\lambda_+(\varepsilon)$ is the transition rate calculated from the mean free path of a nucleon in nuclear matter according to the hybrid model. For the compound nucleus contributions, EMPIRE specific Hauser-Feshbach Statistical Compound Nucleus Model (Hauser and Feshbach, 1952) was used where the contribution of the Compound Nucleus (CN) state to the cross section which also holds for Secondary Compound Nucleus (CNs) formed due to subsequent particle emission is given as:

$$\sigma_{p,x}(E) = \sum_{J\pi} \sigma_p^{CN}(E, J\pi) P_x(E, J\pi) \quad [8]$$

Here, $\sigma_p^{CN}(E, J\pi)$ is the cross section of the compound nucleus formation in a state of spin and parity $J\pi$ associated to the incident channel p and $P_x(E, J\pi)$, represents the decay probability of the compound nucleus with the excitation energy E_x in x channel. The decay probability is defined in terms of transmission coefficients as:

$$P_x(E, J\pi) = \frac{T_x(E_a, J\pi)}{\sum_c T_c(E_a, J\pi)} \quad [9]$$

Also, the transmission coefficient for the x particle emission has the expression:

$$T_x(E, J\pi) = \sum_{I=|J-j|}^{I=J+j} \int_0^{E_p - B_x} \sum_{lj} T_{x,lj} \left(E_p - B_x + \varepsilon\right) \rho(\varepsilon, I\pi_I) \delta(\pi\pi_{I,}(-1)^l) d\varepsilon \quad [10]$$

Here, B_x is the separation energy of particle x in the compound nucleus; $p(\varepsilon, I\pi_I)$ is the density of levels in the residual nucleus with the spin and parity I, π_I and the excitation energy ε; $T_{x,lj}$ is the transmission coefficient having channel energy $E_p - B_x - \varepsilon$ and orbital angular momentum l; and $\delta(\pi\pi_I, (-1)^l)$ is a factor which stands for parity conservation.

Furthermore, to account for the correlation between incident and exit channels in elastic scattering, the HRTW model by Hofmann et al. (1975) which accommodates the statistical model with full gamma-cascade to treat the compound nucleus mechanism, is used, where the Elastic Enhancement Factor Wp is given as:

$$W_p = 1 + 2\left[1 + T_p^F\right]^{-1} + 87 \left(\frac{T_p - T_{pre}}{\Sigma_c T_c}\right)^2 \left(\frac{T_p}{\Sigma_c T_c}\right)^5 \quad [11]$$

The Enhanced Generalized Superfluid Model (EGSM) level density was used to describe the nuclear structures with the low energy region given as

$$\rho\left(E_p, J, \pi\right) = \rho_{qx}(E_a, J, \pi) K_{rot} Q_{rot} K_{vib} Q_{vib} \qquad U \le U_c \quad [12]$$

Finally, the gamma ray strength function is accounted for with the Modified Lorentzian where for a γ - ray emission of multi pole type XL, the γ -decay strength function is defined as

$$f_{XL}\left(E_\gamma\right) = E_\gamma^{-(2L+1)} \langle \Gamma_{XL(E_\gamma)} \rangle / D_1 \quad [13]$$

where $E_{\gamma}^{-(2L+1)}\langle\Gamma_{XL(E_{\gamma})}\rangle$ is the Average Reduced Partial Radiation Width and $D_1$is the Average Level Spacing.

3.0 RESULTS AND DISCUSSION

Results of evaluations carried out with EMPIRE 3.2 are presented in this section from Fig. 1 to Fig 15 with different modelling considerations.

3.1 Dispersive and Relativistic Effects of Proton Incident OMP

Excitation function of the ^{151}Sm(p,n)^{151}Eu reaction presented in Fig 1 demonstrate the effect of dispersive and relativistic consideration in the proton incident OMP on the calculated cross section. The four different proton incident OMPs, as given in Table 1 were employed to describe the proton interaction on the spherical targets and to verify the effect of the dispersiveness or relativity in the calculation of the probability of proton induced direct reactions.

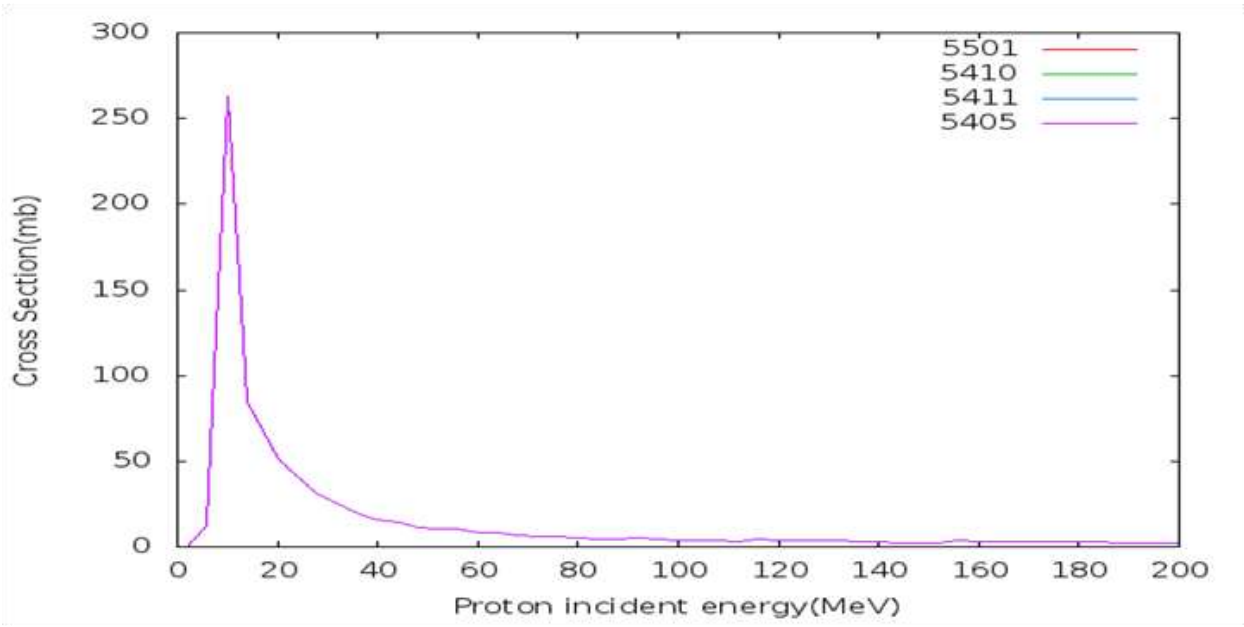

Fig. 1:The comparison of the effect of the proton incident optical model potentials using^{151}Sm(p,n) ^{151}Eu reaction.

As seen in Fig 1, the comparison of the global OMPs for the proton incident channel does not show any variation in the contributions of the OMPs to the calculation of the cross sections This implies that the description of the optical wave as dispersive or relativistic has no effect on the probability of proton induced direct

processes in LLFPs at energies up to 200 MeV.

3.2 Effect of PE Contributions from PCROSSand HMS

For all the LLFP nuclei of interest, only ^{90}Sr, ^{99}Tc and ^{137}Cs have measurements reported for proton induced cross section at energies of relevance to ADS application and close to 200 MeVupper limit for this studies.Fig. 2 to 5 presents the impact of HMS and/or PCROSS PE mechanisms on the cross section of ^{90}Sr(p,n) ^{90}Y, ^{90}Sr(p,2n)^{89}Y and ^{90}Sr(p,3n)^{88}Y bencmarked with the only availablle experimetal measurement of Wang et al. (2016).

From Fig. 2, it is clear that the contribution of the HMS PE mechanism better predicts the single^{90}Sr(p,n)^{90}Y cross section measurement of Wang et al. (2016) available at 185 MeV better than the PCROSS PE mechansim's contribution.

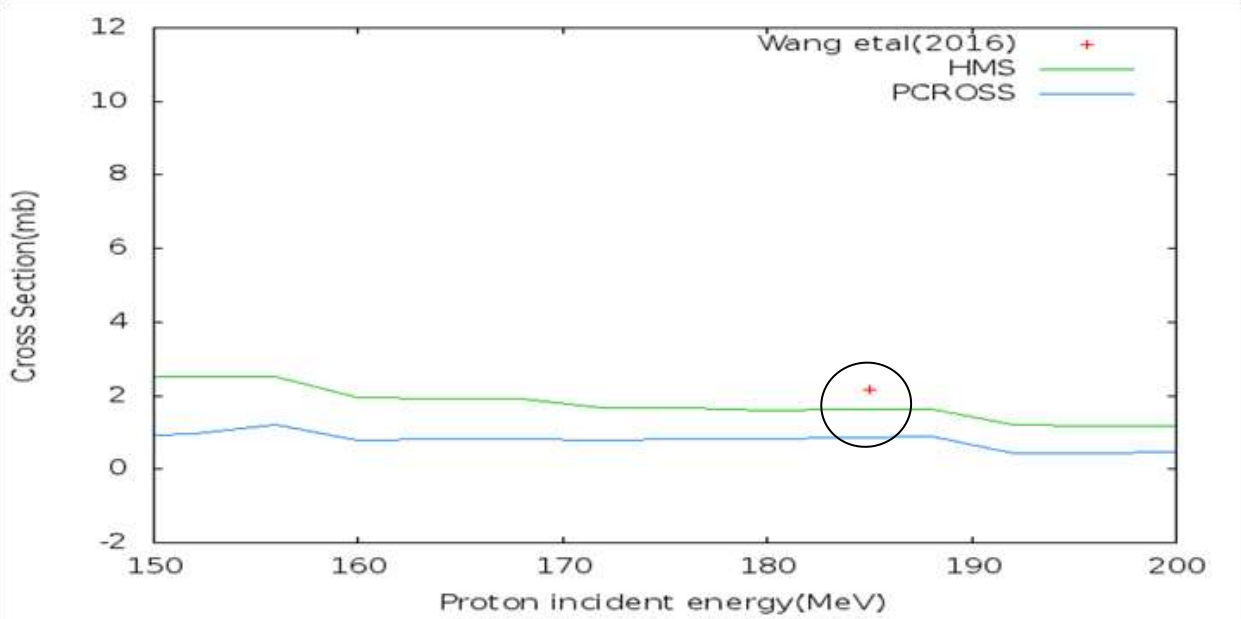

Fig. 2: Excitation Function of ^{90}Sr(p,n)^{90}Y Reaction with PCROSS and HMS PE Contribution Compared with Experimental Datafrom Wang et al. (2016) (Circled) from 150 – 200 MeV

The complete excitation fucntion from 0 to 200 MeV for ^{90}Sr(p,n)^{90}Y reactionis presnetd in Fig. 3showing the peak characteristics and good agreement with Wang et al. (2016) at 185 MeV.

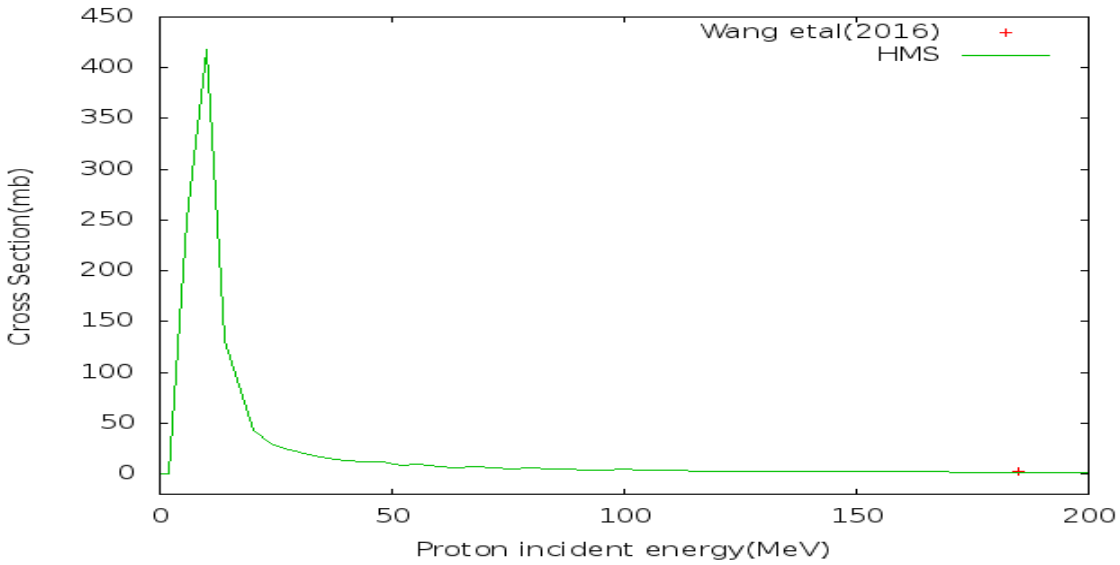

Fig.3:Excitation Function of $^{90}Sr(p,n)^{90}Y$ with HMS PE mechanism contribution from 0-200 MeV showing the peak Cross Section and Energy with Wang et al. (2016) (Circled).

Similarly, Fig. 4 presents both the HMS and PCROSS contributions to the $^{90}Sr(p,2n)^{89}Y$ reaction from 150 – 200 MeV and highlights the better agreement of the HMS PE mechanism with measurement compared with the PCROSS. It is also noted that the disagreement with the measured Wang et al. (2016) cross section for the $^{90}Sr(p,2n)^{89}Y$ reaction at 185 MeVappears to be more significant when compared to the $^{90}Sr(p,n)^{90}Y$ reaction.

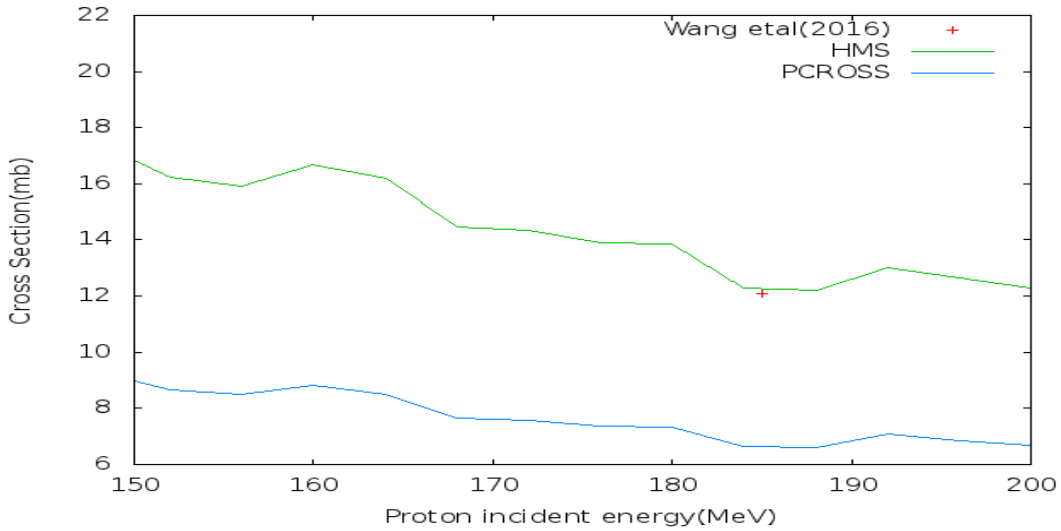

Fig.4: Excitation Function of $^{90}Sr(p,2n)^{89}Y$ Reaction from 150 – 200 MeVwith PCROSS and HMS PE Contribution Compared with Experimental Data from Wang et al. (2016) (Circled)

Furthermore, Fig. 5 presents the HMS and PCROSS PE contribution to the $^{90}Sr(p,3n)^{88}Y$ reaction cross section in comparison with the Wang *et al.* (2016) measurement for the reaction at 185 MeV. The observations with respect to Fig. 4 are also noted here with the HMS PE mechanism showing better agreement and the disagreement of the PCROSS mechansim noted to be more significant than observed in both the $^{90}Sr(p,n)^{90}Y$ and $^{90}Sr(p,2n)^{89}Y$ reactions.

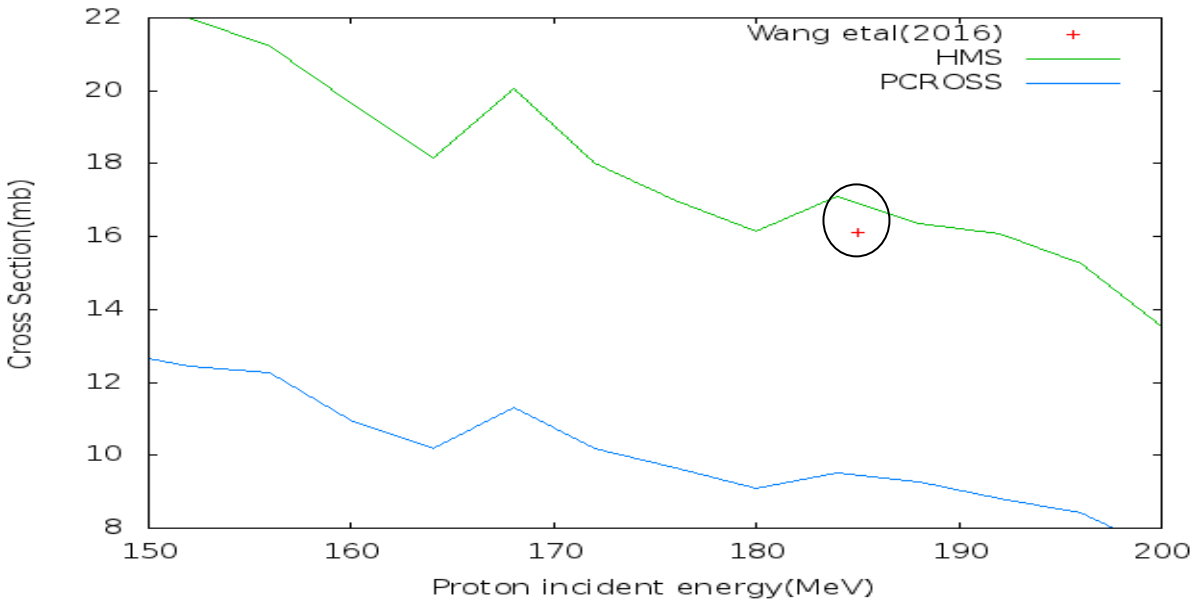

Fig.5: The graph of the cross section of $^{90}Sr(p,3n)^{88}Y$ calculated with PCROSS and HMS along the experimental data (Circled).

Thus, it can be concluded that the HMS PE mechanisms contrbutes to a better description of the proton induced activation of LLFPs at aorund 185 MeV and provides a good assement of the reaction probability for the $^{90}Sr(p,n)^{90}Y$, $^{90}Sr(p,2n)^{89}Y$ and $^{90}Sr(p,3n)^{88}Y$ reaction better than the PCROSS mecahnism. Furthermore, the disagreement of the PCROSS PE mechanism is noted to increase with increasing neutron emission around the same energy. This implies that as number of neutron emitted increases, the performance of the PCROSS mechanism in accounting explicity for the reaction probability reduces.

The better performance of the HMS model can be attributed to its foundation in the Intra-nuclear Cascade (INC) approach found to be effective at higher energy up to 250 MeVby treating all excitons, including holes, on equal footings, giving each of them a chance to interact or to be emitted with a priori equal probability and ending the cascade when all excitons are bound

(Blann and Chadwick, 1998). In contrast to other pre-equilibrium models, this approach avoids multi-exciton level densities which were shown to be used inconsistently in the exciton and in the hybrid formulations. It is also very attractive, due to the lack of physical limit apart from energy conservation, on the number of pre-equilibrium emissions; the inclusion of the linear momentum conservation and the provision of a nearly complete set of observables including the spin and excitation-energy dependent population of residual nuclei, an essential feature for coupling the pre-equilibrium mechanism to the subsequent compound nucleus decay.

3.3 PCROSS PE with Mean Free Path (MFP) Contributions in ^{99}Tc(p,3n)^{97}Ru Reaction

From the different ^{99}Tc reactions of interest, only ^{99}Tc(p,3n)^{97}Ru reaction has available measured cross section dataat energies below 100 MeV as reported by Zaytseva *et al*. (1992). The PCROSS PE mechansim relaibly predicts the trend of the measurement as shown in Fig. 6,7 and 8. In Fig. 6 and 7, uisng PCROSS PE model with Mean Free Path (MFP) values set at 1.5 and 3.0 respectively, it is observed that the higher MFP at 3.0 predicts the measured peak cross section better.

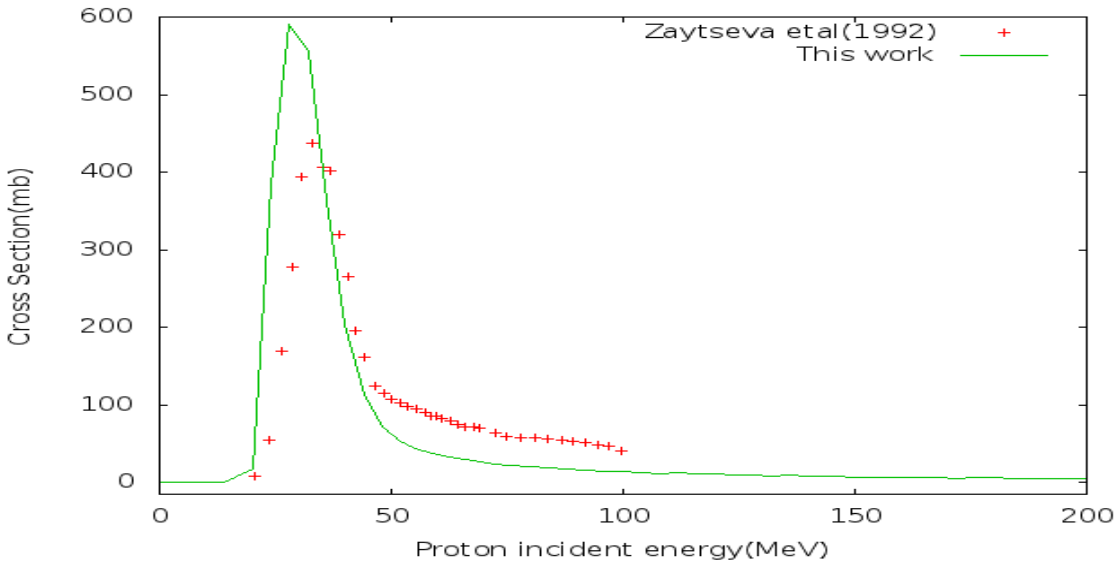

Fig.6:Excitation Function of ^{99}Tc(p,3n)^{97}Ru using PCROSS PE at MFP = 1.5 Contribution with Measurement of Zaytseva et al. (1992)

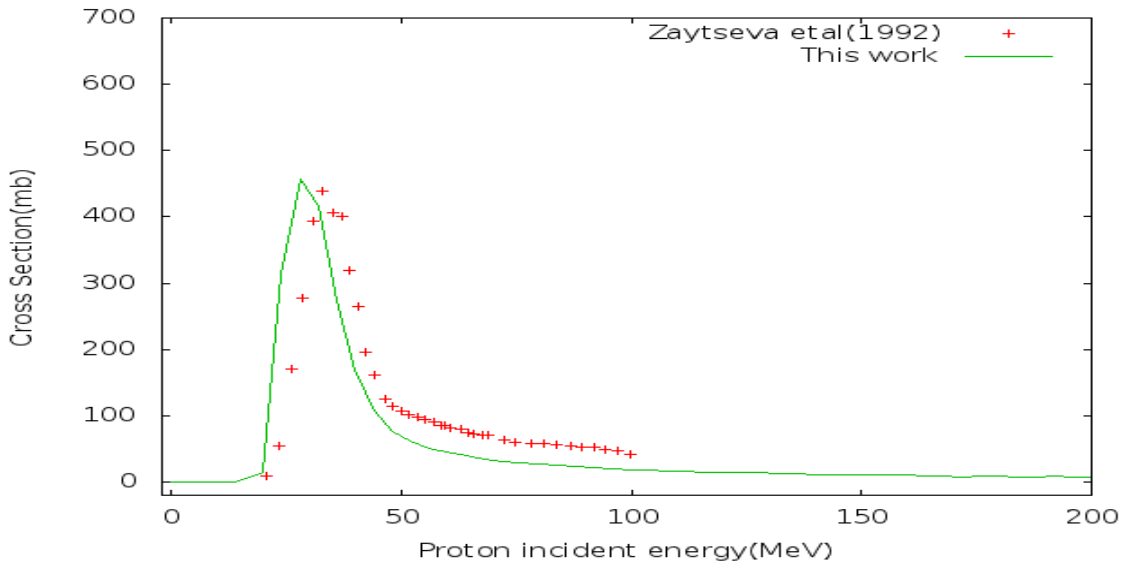

Fig.7: Excitation Function of $^{99}Tc(p,3n)^{97}Ru$ using PCROSS PE at MFP = 3.0 Contribution with Measurement of Zaytseva et al. (1992)

The MFP, which provides the average distance travelled by the proton between successivecollisions that sufficiently modifies its properties, is thus found to play a major role in the better prediction of the proton induced (n,3p) reaction for LLFPs within the PCROS PE mechansim and is seen to reduce the peak cross section at the same energy as it is increased to better describe the measuered data.

3.4 HMS and PCROSS PE Mechanism Contributios above 30 MeV for $^{99}Tc(p,3n)^{97}Ru$

The HMS PE mechanism shows improvement of the prediction of the cross section from about 30MeV and above better than the PCROSS with 1.5 or 3.0 MFP as shown in Fig. 8. The peak cross section predicted is however significantly higher than the available measuered data of Zaytseva et al. (1992) compared with the good agreement observed with PCROSS PE with MFP = 3.0 for the same study. This observation implies that care most be taken to avoid double counting around the peak energy. This feature is an integral part of the Master Equation on which PCROSS is built to be optimal at about 25 MeV (Ribansky, Oblozinsky and Betak, 1973; Cline and Blann, 1972; Cline, 1972; Griffin, 1966).

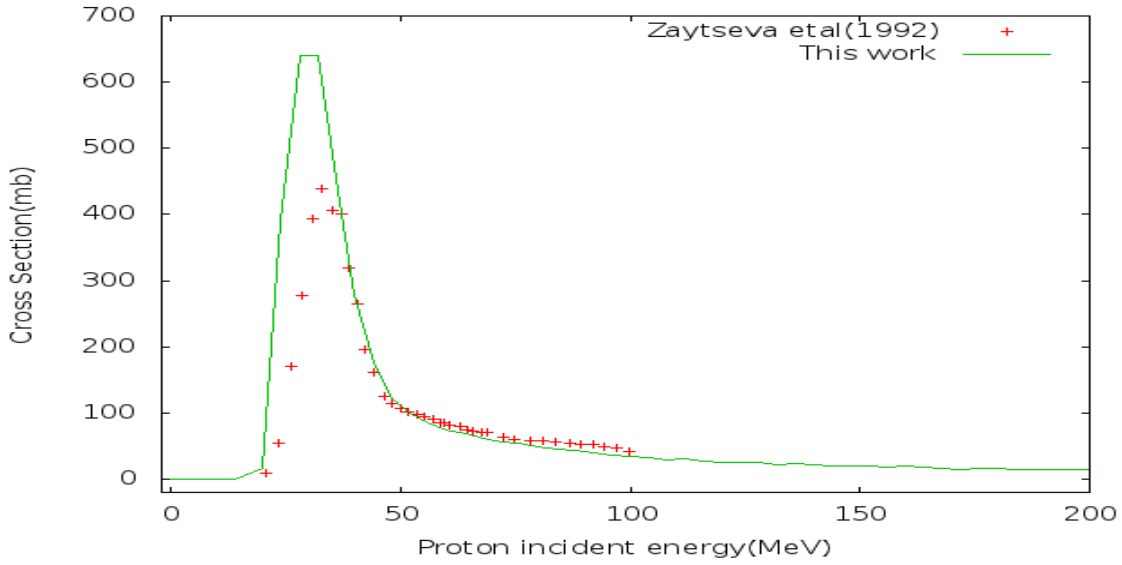

Fig.8:Excitation Function of the cross section of $^{99}Tc(p,3n)^{97}Ru$ calculated with HMS PE Model with Measured Data from Zaytseva et al. (1992)

3.5 Excitation Function of the $^{137}Cs(p,2n)^{136}Ba$ and $^{137}Cs(p,3n)^{135}Ba$ Reactions

Fig. 9 and 10 provides the evaluation for (p,2n) and (p,3n) reactions on ^{137}Cs for which measured values were reported by Wang *et al*. (2016). The PCROSS PE mecahnsim has been found to better predict the high energy end for this reaction as shown in Fig. 9 and Fig.10.

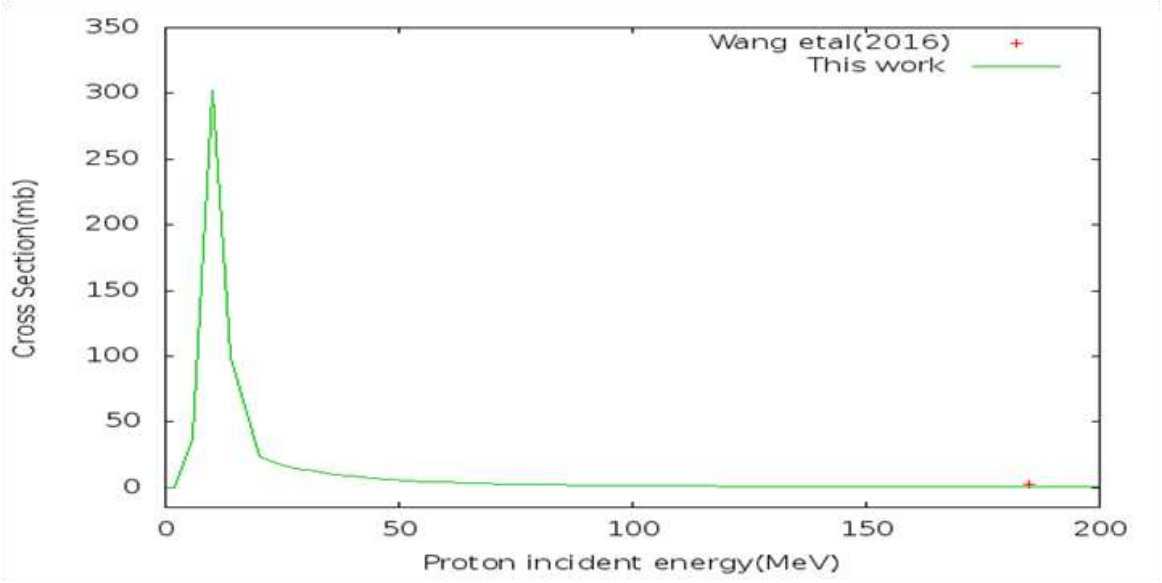

Fig. 9:Excitation Function of the $^{137}Cs(p,2n)^{136}Ba$ reaction calcuated with PCROSS with Measured data from Wang et al. (2016) (Circled).

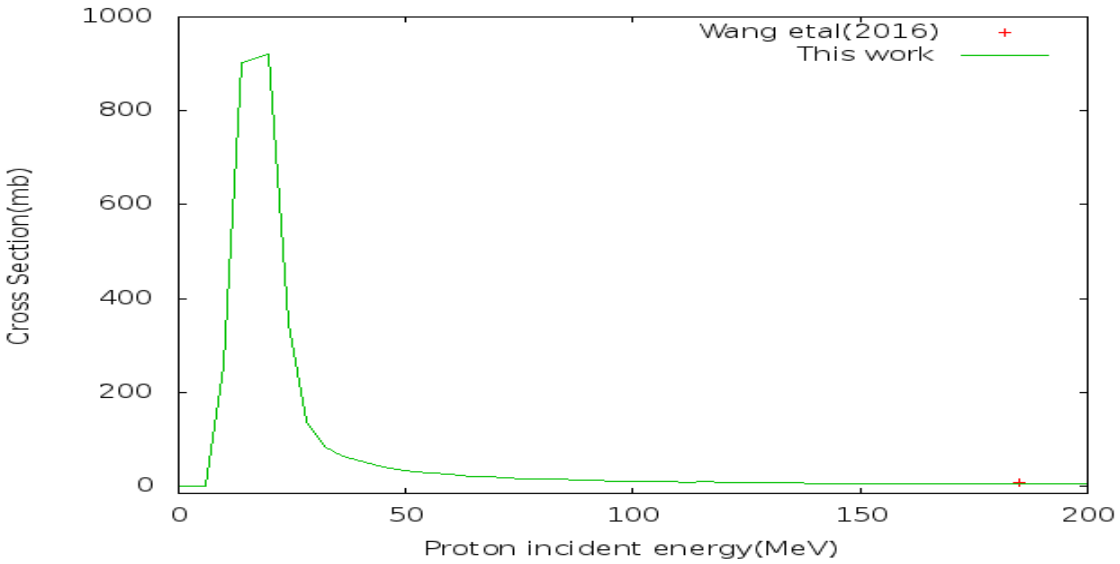

Fig. 10:Excitation Function of the $^{137}Cs(p,2n)^{135}Ba$ reaction calcuated with PCROSS with Measured data from Wang et al. (2016) (Circled).

3.6 Benchmarking with Evaluated Data from TENDL

In the light of scanty measured data, an attempt is made to further verify the calculations of cross section for the LLFPs in this work with the only available evaluated data from the TALYS Based Evaluated Nuclear Data Library TENDL (TENDL, 2009 & TENDL, 2014). As shown in Fig. 10 and 11 for $^{79}Se(p,2n)^{78}Br$ and $^{79}Se(p,3n)^{77}Br$respectively, datafrom this work shows better features of the neutron emission spectrum absent in the two TENDL evaluations. The peak cross section values at corresponding energies, characteristics of neutron emission spectrums, are crucial for the transmutation system design, analysis and energetics.

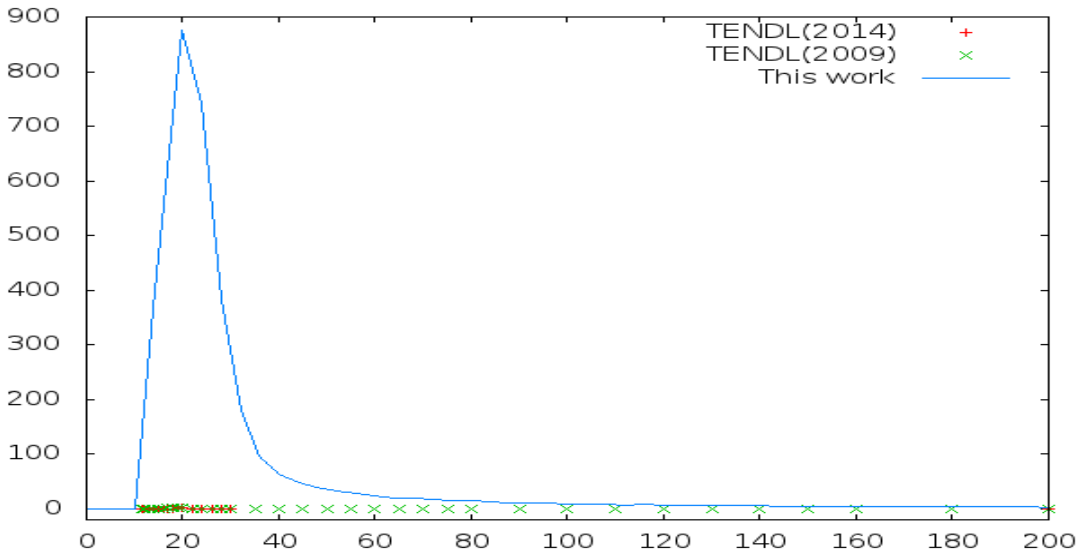

Fig. 11: Benchmarking of calculated $^{79}Se(p,2n)^{78}Br$ Excitation Function with TENDL (2009, 2014) Evaluations

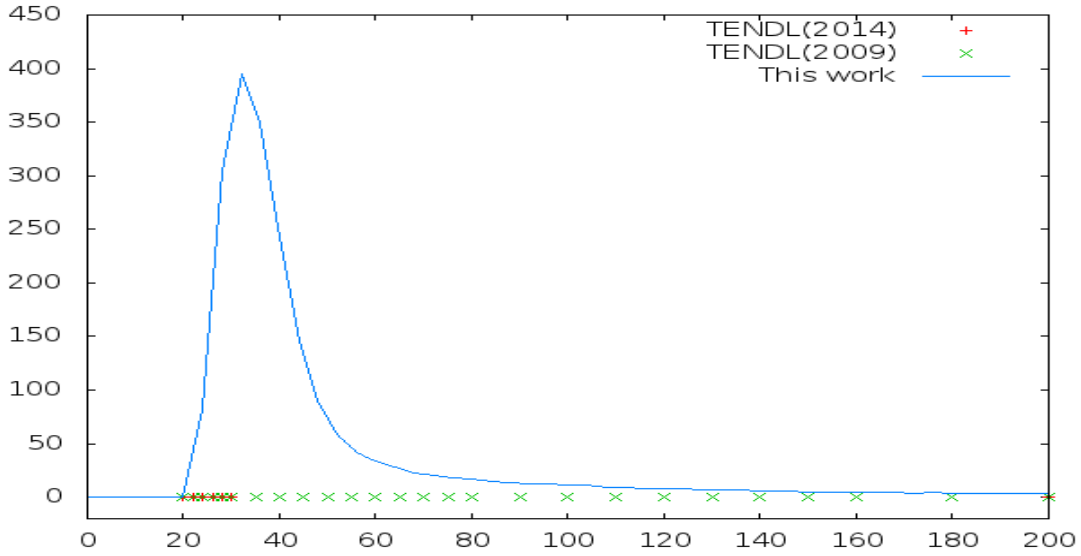

Fig. 12: Benchmarking of calculated $^{79}Se(p,3n)^{78}Br$ Excitation Function with TENDL (2009, 2014) Evaluations

3.7 Peak Values of the (p,n), (p,2n) and (p,3p) Reactions for all LLFPs

The excitation functions of the (p,n), (p,2n) and (p,3n) reactions for the LLFPs are presented in Fig. 13, 14 and 15. Table 2 present the details of the peak cross section at the corresponding energy of peak cross section. It is noted that for all LLFPs, the excitation function for all the nuclei and for all the different reaction channels, only one peak is observed from 0 to 200 MeV similar to the observation for photo-neutron cross

section in spherical nuclei with mass number A > 60 and confirming the spherical sturcture of the nuclei of interest (Brink, 2008).

It is observed that most of the activities of (p, n) reaction take place below 40 MeV as shown in the low cross section above 40 MeV in Fig. 13. Similarly, most of the activities of (p,2n) takes place above 60 MeV as shown in Fig. 14 while most of the activities of (p,3n) take place above 80 MeV as shown in Fig. 15. The implies that this different channels becomes closed at 40, 60 and 80 MeV proton incident energiesrespectively with transmutation possibilities minimizing for all the LLFPs after the closure of the channel.

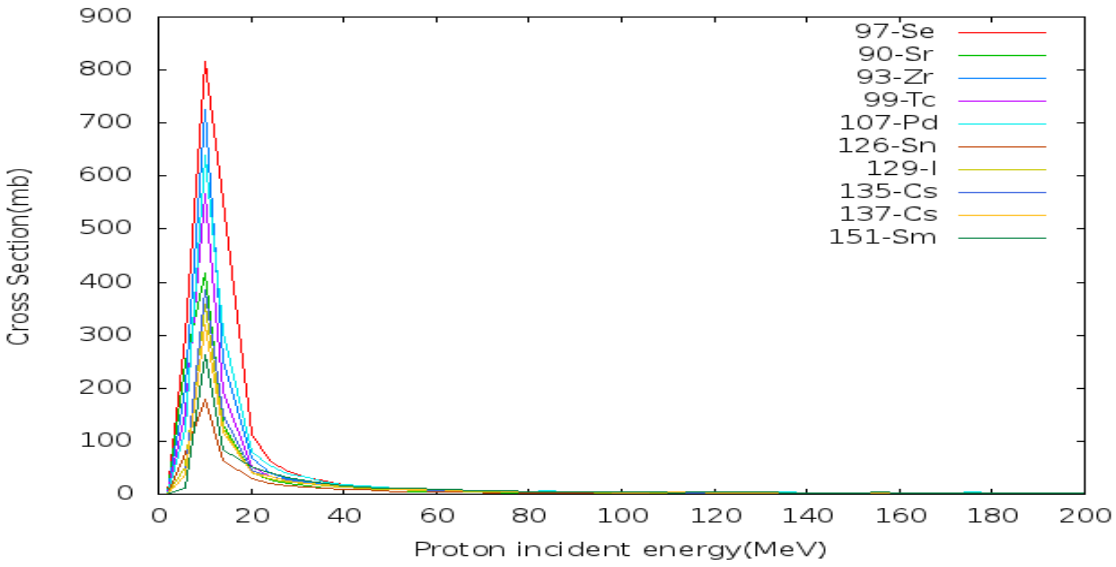

Fig. 13:The (p,n) Reactions Excitation Functions up to 200 MeV for LLFPs with Comparative Peak Cross Sections

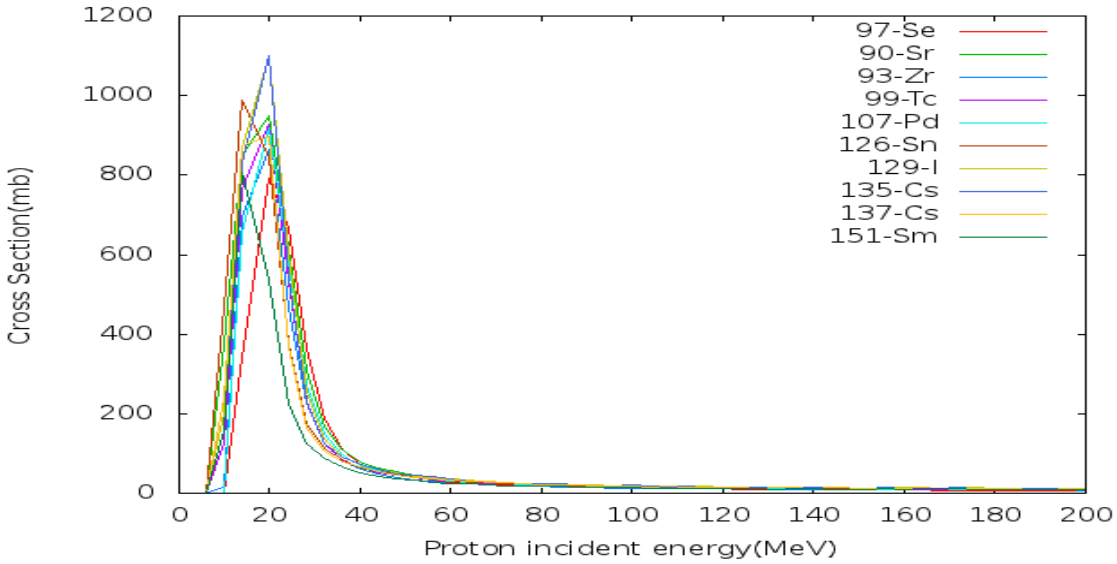

Fig. 14:The (p,2n) Reactions Excitation Functions up to 200 MeV for LLFPs with Comparative Peak Cross Sections

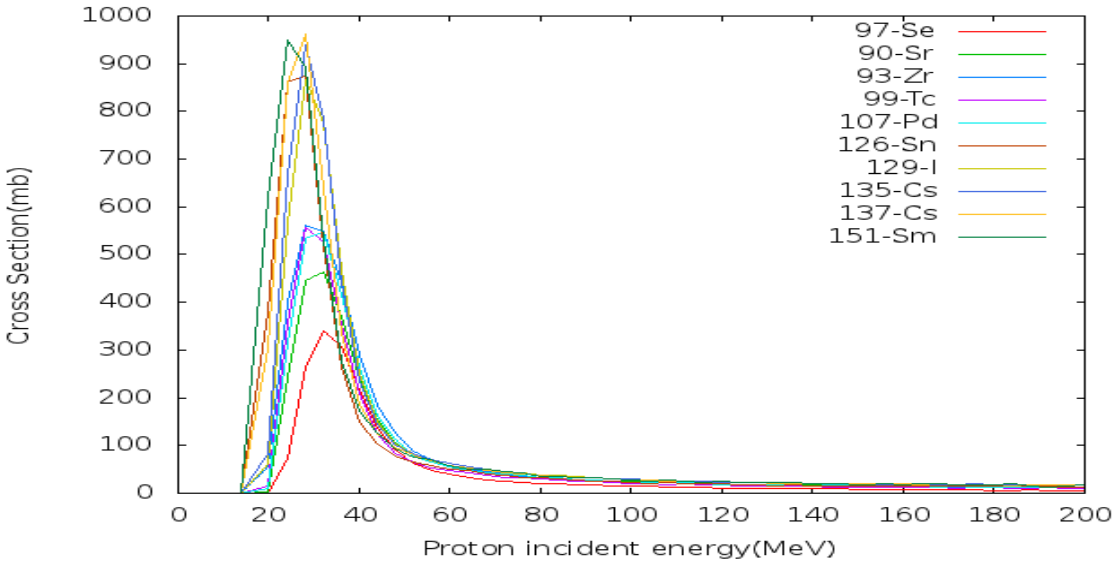

Fig. 15: The (p,3n) Reactions Excitation Functions up to 200 MeV for LLFPs with Comparative Peak Cross Sections

Table 2 provides the transmutation characteristics for the different LLFPs based on the calculated excitation function from this study. It highlights the preferred reaction routes and the energy requirement in an ADS where proton is used to drive the transmutation process. From the table, the (p,n) channel favours the transmutation of ^{79}Se, the (p,2n) channel favors the transmutation of ^{90}Sr, ^{93}Zr, ^{99}Tc, ^{107}Pd, ^{126}Sn, ^{129}I and ^{135}Cs while the (p,3n) channel favors the transmutation of ^{137}Cs and ^{151}S, in an subcritical ADS system.

Table 2: Calculated Peak Cross Section at Corresponding Peak Cross Section Energy for (n,p), (n,2p) and (n,3p) reaction for LLFPs

(n,p)			(n,2p)			(n,3p)		
Reaction	**Peak Energy (MeV)**	**Peak Cross Section (mb)**	**Reaction**	**Peak Energy (MeV)**	**Peak Cross Section (mb)**	**Reaction**	**Peak Energy (MeV)**	**Peak Cross Section (mb)**
^{79}Se(p,n)^{79}Br	9.85428	816.806	^{79}Se(p,2n)^{78}Br	20.0546	793.819	^{79}Se(p,3n)^{77}Br	32.0765	345.529
^{90}Sr(p,n)^{90}Y	10.0728	420.352	^{90}Sr(p,2n)^{89}Y	20.1457	952.818	^{90}Sr(p,3n)^{88}Y	32.0173	467.682
^{93}Zr(p,n)^{93}Nb	9.92996	727.082	^{93}Zr(p,2n)^{92}Nb	19.8599	865.523	^{93}Zr(p,3n)^{91}Nb	28.0167	562.017
^{99}Tc(p,n)^{99}Ru	10.0728	568.259	^{99}Tc(p,2n)^{98}Ru	19.7860	929.152	^{99}Tc(p,3n)^{97}Ru	28.0601	559.385
^{107}Pd(p,n)^{107}Ag	10.0000	639.396	^{107}Pd(p,2n)^{106}Ag	19.9815	921.451	^{107}Pd(p,3n)^{105}Ag	32.1811	550.843
^{126}Sn(p,n)^{126}Sb	10.0000	181.790	^{126}Sn(p,2n)^{125}Sb	14.0665	987.662	^{126}Sn(p,3n)^{124}Sb	28.1146	878.338
^{129}I(p,n)^{129}Xe	10.0000	360.581	^{129}I(p,2n)^{128}Xe	19.9815	1095.24	^{129}I(p,3n)^{127}Xe	28.1146	870.342
^{135}Cs(p,n)^{135}Ba	10.0000	386.819	^{135}Cs(p,2n)^{134}Ba	19.9815	1102.73	^{135}Cs(p,3n)^{134}Ba	28.1146	941.559
^{137}Cs(p,n)^{137}Ba	10.0000	319.225	^{137}Cs(p,2n)^{136}Ba	19.9815	903.327	^{137}Cs(p,3n)^{135}Ba	28.1146	962.674
^{151}Sm(p,n)^{151}Eu	10.0000	263.002	^{151}Sm(p,2n)^{150}Eu	14.0665	806.497	^{151}Sm(p,3n)^{149}Eu	24.0481	956.427

4.0 CONCLUSION

The results of (p,n), (p,2n) and (p,3n) reaction cross-sections of LLFPs provides significant nuclear data input in the context of the scanty data available across the wide energy range of interest. The result reveals that the models used are quite suitable in predicting the reaction cross-section with proton energy up to 200MeV. These OM, OMP, PE and CN models and parameters as implemented for the study gave results in good agreement with standard EXFOR cross section data. The result shows that the description of the optical wave as dispersive or relativistic has no effect on the calculated cross section. The HMS PE model, which avoids multi exciton and accounts for linear momentum conservation, was observed to have contributed better in describing the available measured data especially above 30 MeV beyond the reactor energy spectrum of 20 MeV. The MFP at 3.0, which extend the distance considered within collision of significance, was also noted to improve the description of the measured data for the peak cross section within the PCROS mechanism. The singular peak for each channel from 0 -200 MeV further confirms the sphericity of the nuclei. These characteristics confirm known theories.

The results presented here shows significant improvement in comparison with the available TENDL evaluations and shows more consistency with the measured data especially around the neutron emission spectrum of peak cross sections. This study therefore presents a new consistent cross section data for LLFP isotopes ^{79}Se, ^{90}Sr, ^{93}Zr, ^{99}Tc, ^{107}Pd, ^{126}Sn, ^{129}I, ^{135}Cs, ^{137}Cs and ^{151}Smfall within good margin of available data and are expected to serve as improved input for ADS design.

REFERENCES

Blann M. and Chadwick, M.B. (1998), *New Pre-Compound Decay Model: Angular Distributions,* Physical Review C Volume 54, p.l341

Brink D. M. (2008),*Giant Resonances in Excited Nuclei*, Talk presented at the workshop on Chaos And Collectivity in Many Body System' at the PMIPKS, Dresden, Germany.

Capote, R., Herrera, E., Lopez, R. and Osorio, V. and Piris, M. (1991), *Analysis of Experimental*

Data on Neutron Induced Reactions and Development of PCROSS Code for the Calculation of the Differential Preequilibrium Spectra, Final Report of Research Contract 5472/RB, INDC-IAEA,

Carlson B. V. (2002), *A Brief Overview of Models of Nucleon Induced Reaction,* ICTP Lecture Note, Trieste, Volume. 12.

Chadwick M. B., Young P. G., George D. C. and Watanabe Y. (1994), *Multiple Preequilibrium Emission in Feshbach-Kerman-Koonin Analyses*, Physical Review C 50 Issue 2, pp. 996-1005

Cline C. K. and Blann M. (1972), *The Pre-Equilibrium Statistical Model: Description of the Nuclear Equilibration Process and Parameterization of the Model,* Nuclear Physics A 172, pp. 225-259.

Cline C K (1972), *Extension to the Pre-Equilibrium Statistical Model and a Study of Complex Particle Emission,* Nuclear Physics A Volume 193, pp.417-437.

Ribansky I., Oblozinsky P., and Betak E. (1973), *Pre-Equilibrium Decay and the Exciton Model,* Nuclear Physics A Volume 205, pp. 545-560.

European Commission, (2001). *Partitioning and Transmutation: Towards an easing of the Nuclear Waste Management Problem*. European Commission Research Directorate-General Communication Unit Rue de la Loi/Wetstraat 200, ISBN 92-894-1074-4).

Griffin J. J. (1966), *Statistical Model of Intermediate Structures,* Physical Review Letters Volume 17, pp. 478-481.

Hauser W. and Feshbach H. (1952). *Angular Momentum and Parity Conservation Consideration in the Analysis of Equilibrated Statistical Processes*, Physical Review A Volume 87, p.366.

Hofmann H.M., Richert J., Tepel, W. and Weidenmuller H. A. (1975). *Direct Reactions and Hauser-Feshbach Theory*, Annals of Physics 90, pp.403-437.

Hofmann H. M., Mertelmeier T., Herman M., Tepel 1. W., (1980), *Hauser-Feshbach calculations in the presence of weakly absorbing channels with special reference to*

the elastic enhancement factor and the factorization assumption, Zeitschrift fur Physik A, Atoms and Nuclei 297 (2), 153-160.

IAEA (2015), *Status of Accelerator Driven Systems Research and Technology Developmen*t, IAEA-TECDOC-1766

Ikeda, Y., (2002) *Nuclear Data Relevant to Accelerator Driven System*, Journal of Nuclear Science and Technology, *39:*sup2, pp. 13-18.

Koning A.J. and Delaroche J.P. (2003), *Local and global nucleon optical models from 1 keV to 200 MeV*. Nuclear Physics A 713 P 231–310.

Makinaga A., Aikawa M., Kato K., Kohoma A., Otsu H., and Sakurai. (2014) *Systematic Study of Nuclear Data for Nuclear Transmutation*. RIKEN Accel. Prog. 47, Faculty of Science, Hokkaido University.

Morillon B. and Romain P. (2007) *Bound single-particle states and scattering of nucleons on spherical nuclei with a global optical model*. Physical Review C76, 044601 (2007).

Raynal J. (1972), *Optical Model and Coupled Channel Calculations in Nuclear Physics*, Computing as a Language of Physics, ICTP International Seminar Course, IAEA/ICTP, Trieste, Italy August 2-10 1971,p. 281.

Satoshi Chiba, Toshio Wakabayashi, Yoshiaki Tachi, Naoyuki Takaki, Atsunori Terashima, Shin

Okumura and Tadashi Yoshida (2017), *Method to reduce long-lived fission products by nuclear transmutations with fast speed reactor*, Scientific Reports 7:13961.

Shubin, Yu. N., Lunev, V.P., Konobeyev, A. Yu and Dityuk, A. I. (1995)*Cross-Section Library MENDL-2 to Study Activation and Transmutation of Materials Irradiated by Nucleons of Intermediate Energies*, IAEA Report No. INDC(CCP)-385.

Soukhovitskii E. S. , Morogovskij G. B., Chiba S. and Fukahori T. (2004), *Physics and Numerical Methods of OPTMAN A Coupled-Channels Method Based on Soft-Rotator Model for a Description of Collective Nuclear Structure and Excitations,* Technical Report, JAERI-Data/Code 2004-002, Japan Atomic Energy Research Institute

Soukhovitskii E. S., Chiba S., Iwamoto 0., Shibata K., Fukahori T., Morogovskij G. B.(2005), *Programs OPTMAN and SHEMMAN Version 8,* Technical Report No. JAERIData/Code 2005-002, Japan Atomic Energy Research Institute.

Soukhovitskii E. S., Chiba S., Capote R., Quesada 1. M., Kunieda S., Mororovskij G. B. (2008), *Supplement to OPTMAN Code, Manual Version 10,* Technical report, JAERIData/Code 2008-025, Japan Atomic Energy Research Institute.

TENDL (2014), Se-79(p,2n)Br-78, SIG. ftp://ftp.nrg.eu/pub/www/talys/tendl-2014/proton_file /Se/079/lib/endf/Se079-p.tendl. Retrieved on 10 Oct June, 2020.

TENDL (2009), Se-79(p,2n)Br-78, SIG. ftp://ftp.nrg.eu/pub/www/talys/tendl-2009/proton_file /Se /079/lib/endf/Se079-p.tendl. Retrieved on 10 Oct, 2020.

Xiaohua Li, Chonghai Cai.(2008) *Global dispersive optical model potential for proton as projectile in the energy region up to 200 MeV*, Nuclear Physics, Section A, Volume 801, Issue 1, p. 43-67.

Wang H., Otsu H., Sakurai H., Ahn D.S., Aikawa M., Doornenbal P., Fukuda N., Isobe T., Kawakami S., Koyama S., Kubo T., Kubono S., Lorusso G., Maeda Y., Makinaga A., Momiyama S., Nakano K., Niikura M., Shiga Y., Soderstrom P.-A., Suzuki H., Takeda H., Takeuchi S., Taniuchi R., Watanabe Ya., Watanabe Yu., Yamasaki H., Yoshida, K (2016) *Spallation reaction study for fission products in nuclear waste: Cross section measurements for 137Cs and 90Sr on proton and deuteron*, Physics Letters, Section B, Vol.754, p.104.

Yang W. S., Kim Y., Hill R. N., Taiwo T. A., and Khalil H. S. (2004) *Long-Lived Fission Product Transmutation Studies.* Nuclear Science and Engineering: 146, pp. 291–318

Zaytseva N.G., Rurarz E., Vobecky M.,Kim Hyn Hwan, Nowak K., Tethal T., Khalkin V.A., Popinenkova L.M. (1992) *Excitation Function and Yield For Ru-97 Production In Tc-99(P,3N)Ru-97 Reaction in 20-100 MeV Energy Range*, Radiochimica Acta, Vol.56, p.59